

# Approach for composition measurement of cosmic rays using muon-to-electron ratio observed by LHAASO-KM2A

Xishui Tian,<sup>1</sup> Zhuo Li,<sup>1,2,\*</sup> Quanbu Gou,<sup>3,4,5,†</sup> Hengying Zhang,<sup>6</sup>  
Huihai He,<sup>3,4,5</sup> Cunfeng Feng,<sup>7</sup> and Giuseppe Di Sciascio<sup>8</sup>

<sup>1</sup>*Department of Astronomy, School of Physics, Peking University, Beijing 100871, China*

<sup>2</sup>*Kavli Institute for Astronomy and Astrophysics, Peking University, Beijing 100871, China*

<sup>3</sup>*Key Laboratory of Particle Astrophysics, Institute of High Energy Physics, Chinese Academy of Sciences, Beijing 100049, China*

<sup>4</sup>*University of Chinese Academy of Sciences, Beijing 100049, China*

<sup>5</sup>*Tianfu Cosmic Ray Research Center, Chengdu 610000, Sichuan, China*

<sup>6</sup>*School of Physics and Astronomy, Yunnan University, 650091 Kunming, Yunnan, China*

<sup>7</sup>*Key Laboratory of Particle Physics and Particle Irradiation (MOE), Institute of Frontier and Interdisciplinary Science, Shandong University, Qingdao, Shandong 266237, China*

<sup>8</sup>*INFN - Roma Tor Vergata, Via della Ricerca Scientifica 1, 00133 Rome, Italy*

(Dated: July 19, 2024)

Composition measurement of cosmic rays (CRs) around the knee of the CR energy spectrum is crucial for studying the processes of particle acceleration and propagation of Galactic CRs. The Square Kilometer Array (KM2A) of Large High Altitude Air Shower Observatory (LHAASO) can provide precise measurement of the muonic and electromagnetic (em.) components in CR-induced extensive air showers, and hence a good chance to disentangle the CR composition. Here we propose an approach of decomposing CR compositions with the number ratio between muons and em. particles ( $N_\mu/N_e$ ) observed by LHAASO-KM2A: we reconstruct the energy spectra of individual CR compositions by fitting  $N_\mu/N_e$  distributions in each reconstructed energy bin using the template shapes of  $N_\mu/N_e$  distributions of individual CR compositions based on Monte Carlo (MC) simulation. We evaluate the performance of this approach with MC tests where mock data of LHAASO-KM2A are generated by MC simulation. We show that the input composition model can be well recovered in this approach, independent of the CR composition model adopted in the MC simulation for the template distributions. The uncertainties of the reconstructed spectra at  $< 20$  PeV, mainly limited by simulation statistics, are  $\leq 7\%$  for proton, He, and Fe groups, and  $\leq 8\%$  and  $\leq 16\%$  for CNO and MgAlSi groups, respectively.

## I. INTRODUCTION

Cosmic rays (CRs) are high energy atomic nuclei of astrophysical origins. The observed all-particle energy spectrum of CRs is approximately a power-law from GeV to beyond  $10^{11}$  GeV with several breaks where the indices of the power-law change. The energy spectrum of CRs steepens around 4 PeV, with the power-law index changing from  $-2.7$  to  $-3.1$  [1], which is the so-called “knee” of the CR spectrum. The physical cause of the CR spectral knee is still unclear, although many possible reasons had been discussed. First, the break may arise from the particle acceleration capability of Galactic CR accelerators [2, 3], i.e., the maximum energy of CRs that the accelerators can produce. For example, supernova remnants (SNRs) are well discussed to be potential candidates of Galactic CR accelerators [4], which are believed to accelerate protons up to  $\sim 100$  TeV by shock acceleration [5], but hardly up to PeV range [6]. Secondly, the knee may be caused by propagation effects [7–9]. CRs propagate diffusively in the Galactic magnetic field (GMF)

[10, 11]. The propagation process depends on particle energy. Low and high energy CRs follow different propagation patterns, which may lead to a spectral break in between.

Either particle acceleration or propagation process is expected to be governed by electromagnetic (em.) interaction with the background magnetic field, which is rigidity dependent, i.e., the particles with the same rigidity may undergo the similar acceleration and/or propagation processes. Rigidity-dependent spectra are expected for different types of nuclei [12, 13]. Therefore, precise measurements of elemental composition around the knee are crucial to understanding the acceleration and propagation of CRs, and deciphering the mechanism accounting for the knee.

Because of the low CR flux at high energies, CRs of  $> 100$  TeV are detected via extensive air showers by ground-based detectors. Due to the fluctuations in air showers, it is hard to reconstruct the primary mass for single air shower event. However, elemental energy spectra grouped by CR mass can be statistically reconstructed from observables on the ground. Observationally, it is common to decompose the CR compositions at  $> 100$  TeV into five groups, following the direct measurements, proton, He, CNO, MgAlSi, and Fe [14].

Many ground-based experiments had tried to measure

\* zhuo.li@pku.edu.cn

† gouqb@ihep.ac.cn

the CR compositions around the knee region. But the results among experiments are inconsistent, in particular, on the breaks of proton and He spectra. KASCADE decomposed the primary CRs from 1PeV to 100PeV into five mass groups, represented by proton, He, C, Si, and Fe, by unfolding the distribution of secondary electrons and muons [15]. The reconstructed spectra of proton and He break beyond PeV, which indicates the knee of the all particle spectrum results from the breaks of proton and He, namely the light component. On the contrary, a light knee below PeV is observed by Tibet AS $\gamma$  [16] and ARGO-YBJ plus Wide Field Cherenkov Telescope (WFCT) [17] measurements. Tibet AS $\gamma$  measured the energy spectra of proton and He from 1PeV to 10PeV using artificial neural network to reconstruct the primary mass and select proton-like events and light-like events [16]. The spectra of proton and He are expressed as  $E^{-3}$  power-law from 1PeV to 10PeV, suggesting the light component breaks below 1 PeV. ARGO-YBJ+WFCT measured the energy spectrum of proton plus He by selecting light-like events with a two-dimension cut applied to observables from surface detectors and the Cherenkov telescope. The spectrum of light nuclei measured by ARGO-YBJ+WFCT breaks around 700 TeV [17], which is compatible with the results from Tibet AS $\gamma$ , but at odds with the KASCADE measurements.

The inconsistency on the CR composition may come from the limitations of each experiment. For KASCADE, the detectors are deployed at the sea level (grammage  $\sim 10^3$  g cm $^{-2}$ ), which is far from the shower maximum of PeV energies ( $X_{\text{max}} \sim 600$  g cm $^{-2}$ ). Therefore, the measurement suffers more uncertainty from the atmospheric absorption. On the other hand, though located around the shower maximum of PeV showers, Tibet AS $\gamma$  and ARGO-YBJ lack good muon measurements in the shower, which is crucial to distinguishing different nuclei. Thus, an observatory at high altitude as well as having good measurements of secondary muons is necessary to settle the question of the composition around the knee.

The Large High Altitude Air Shower Observatory (LHAASO) [18], with an array area of  $\sim 1.3$  km $^2$  and located at Mountain Haizi, Daocheng, China of 4410 m above sea level, is designed for precise measurements of high energy CR and gamma-ray induced air showers. It consists of three sub-arrays – Square Kilometer Array (KM2A), Water Cherenkov Detector Array (WCDA), and Wide Field Cherenkov Telescope Array (WFCTA) – and observes air showers from high energy CRs and gamma-rays using hybrid techniques [18]. In one of the key goals for CR observations, LHAASO aims to measure the energy spectra, i.e., the spectral knee, of the light (proton or H+He) and Fe groups, by using multiple observables from KM2A, WFCTA and WCDA data combined to select air shower events for individual groups with high purity [19–21].

We note that LHAASO-KM2A can be very powerful for CR composition measurement around the knee region. First, the high altitude of LHAASO, near the shower

maximum for CR energy around 4PeV allows the energy reconstruction of primary CRs with less dependence on the CR composition [22]. The insensitiveness of energy reconstruction to the primary mass will greatly facilitate composition studies. Second, thanks to the dense arrangement of secondary detectors in LHAASO-KM2A, precise measurement of lateral distribution of secondaries in air showers is allowed, and low energy CRs can be observed down to 30 TeV. Third, the large area makes LHAASO-KM2A capable of observing CR with energies up to 100PeV. The wide energy range of CRs observed by LHAASO-KM2A will provide complementary measurements between direct measurements of low-energy CRs via satellites/balloons and high-energy CR observations by ground arrays. Forth, LHAASO-KM2A is equipped with two types of detectors to probe both the muonic and em. components of the shower, which is crucial for mass separation in the composition reconstruction [23].

In this work, we propose an approach of composition measurement by LHAASO-KM2A. Given the measurements of the muonic and em. components of air showers, we use the number ratio between muons and em. particles ( $N_{\mu}/N_e$ ) of the air shower as the mass indicator of primary CRs to reconstruct the elemental energy spectra. We carry out detection simulation to evaluate the performance of LHAASO-KM2A in reconstructing the elemental energy spectra. The paper is organised as follows: Section II introduces the detector layout of LHAASO-KM2A and the detection simulation used in this analysis. Section III describes the analysis procedure, including the energy reconstruction, the mass separation, and the reconstruction of elemental energy spectra. Section IV demonstrates the capability of reconstructing the elemental energy spectra with Monte Carlo (MC) tests and presents the uncertainties in reconstruction shown in the MC tests. Section V is summary and discussion on the approach.

## II. EXPERIMENT AND SIMULATION

### A. LHAASO-KM2A layout

Hybrid techniques for air shower observations are used in LHAASO-KM2A, which consists of 5216 em. detectors (ED) and 1188 muon detectors (MD), independently measuring the secondary particles in the air shower. ED is scintillator detector with a sensitive area of 1 m $^2$ . EDs are deployed over a circle of radius 635 m. The spacing between EDs is 15 m in the central region (with radius  $R < 575$  m) and 30 m at outskirts ( $575 < R < 635$  m). The different spacing is used to better reconstruct the events for showers near the edge of the central array. MD is water Cherenkov detector that has an area of 36 m $^2$  buried under 2.5 m soil to shield it from the electromagnetic particles in the shower. MDs are deployed in the central region of radius 575 m with a spacing of 30 m. Details about the design and performance of ED and MD

can be found in [24].

### B. Detection simulation

In order to evaluate the KM2A performance in composition observations, we carry out MC simulation for the detection. We simulate the interactions and propagation of air showers in the atmosphere and the detector response on the ground. The simulated CR showers are reconstructed by utilising the hit information of the triggered detectors.

In the simulation, five types of nuclei are used: proton, He, N (denoted by CNO), Al (denoted by MgAlSi), and Fe. The shower energy is sampled from a  $E^{-2}$  power-law from 10 TeV to 50 PeV. The incident directions are drawn from an isotropic distribution in the range of zenith  $0-40^\circ$  and azimuth  $0-360^\circ$ .

The simulation is produced by CORSIKA 7.7410 [25] and G4KM2A [26], for air show simulations and detector response, respectively. CORSIKA samples the generation of secondary particles in the atmosphere and the propagation of the shower to the ground. The selected interaction models are QGSJetII-04 [27] for high energy ( $> 80$  GeV) interactions and FLUKA [28] for low energy ( $< 80$  GeV) interactions. The atmosphere model used for CORSIKA is the US standard atmosphere, with a gram-mage of  $597 \text{ g cm}^{-2}$  for the LHAASO site. The magnetic field is set to  $B_x = 34.6 \mu\text{T}$  and  $B_z = 36.1 \mu\text{T}$ , where the x-axis points to the north and the z-axis points vertically downwards.

In the detector response simulation with G4KM2A, the shower cores of the injected showers are uniformly distributed in an annulus  $260 < R < 480$  m from the array center in order to boost sampling efficiency considering the current event selection condition (See Appendix A). In G4KM2A, one CORSIKA shower is reused 20 times to increase the statistics, i.e., a same shower is injected 20 times with different shower core positions. The total number of simulated showers of all five mass groups are around  $5.555 \times 10^7$  before trigger, of which  $1.36 \times 10^6$  events survive after the trigger and event selections.

The trigger events in the simulation are further being reconstructed. The hit information after filtering the noise from triggered detectors is translated into the properties of the primary particle. The shower core position and the incident direction is fitted by the hits from all triggered EDs. The time resolution of ED during reconstruction is set to 0.2 ns. from the charges collected by the EDs (MDs).

## III. CR DECOMPOSING METHOD

Observations of CR compositions call for at least two orthogonal measurements of an air shower to obtain primary energy and mass at the same time. High energy CR particle interacts with nuclei in the atmosphere and

produces secondary mesons, which further decay or interact during propagation. Thus a high energy CR particle will initiate a particle cascade made up of decay and interaction in the atmosphere. Most of the secondary particles that reach the ground are em. particles, including electrons/positrons and photons, and muons. em. particles are mostly resulted from the decay of neutral pions, while muons are from the decay of charged pions. The secondary em. particles and muons are related to the shower development which depends on the energy and mass of the primary CR particle. Therefore, taking advantage of the large and uniform coverage of EDs and MDs of LHAASO-KM2A, we can use the number of em. particles,  $N_e$ , and the number of muons,  $N_\mu$ , of each shower to estimate the CR energy and composition<sup>1</sup> and hence reconstruct the elemental energy spectra.

The proposed method is as follows. First, we reconstruct the shower energies using a composition insensitive method, and then bin events by reconstructed energies. Next, taking advantages of the mass-dependent  $N_\mu/N_e$  ratio, we decompose CR compositions by fitting the  $N_\mu/N_e$  distribution in each reconstructed energy bin. See below for the details.

### A. Mass-insensitive energy reconstruction

The primary CR energy can be given by summing up the two components of CR showers, i.e., em. and muonic components. The altitude of the LHAASO site is around the shower maximum for the knee-region CRs. The proximity to the shower maximum improves the energy reconstruction, and weakens the dependence on the primary CR composition. An approach for energy reconstruction of LHAASO-KM2A has been given in Ref. [22], which is only weakly dependent on the primary mass. For this analysis, we use Eq 9 in Ref. [22] to reconstruct the primary CR energy  $E$ , i.e.,

$$\log(E/\text{GeV}) = 2.768 + \log(2.8N_\mu + N_e). \quad (1)$$

The resolution of energy reconstruction is better than 15% above 300 TeV and the energy bias is smaller than 5% [22], independent of the primary mass.

### B. Mass dependence of $N_\mu/N_e$ ratio

The primary mass affects the properties of air showers, and hence the observables on the ground. For CRs of the same energy, heavy nuclei tend to produce more muons and less em. particles than light nuclei at the shower

<sup>1</sup> Note,  $N_\mu$  and  $N_e$  are the numbers of secondary particles detected by all triggered MDs and EDs located 40–200m from the shower core on the shower plane, respectively.

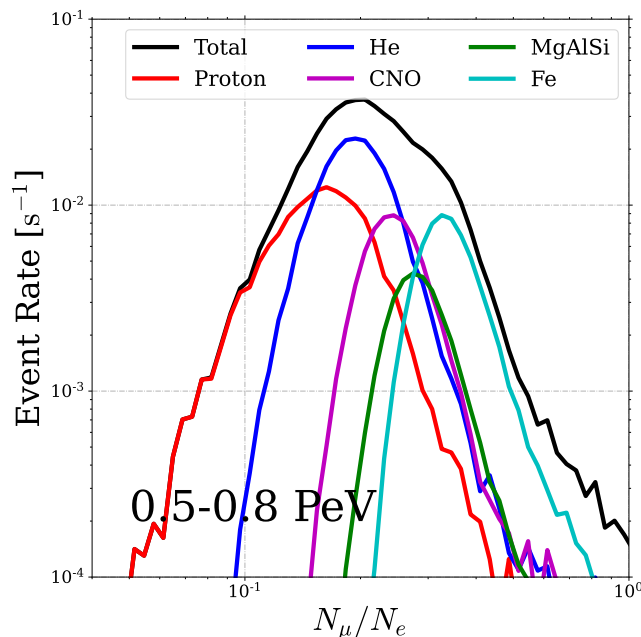


FIG. 1: Simulated  $N_\mu/N_e$  distribution in the reconstructed energy bin of 0.5–0.8 PeV, assuming the H3a model [31]. The black line is the total distribution and the colorful lines are distributions of each mass groups as annotated in the figure legend.

maximum [29]. Therefore,  $N_\mu/N_e$  can be a good estimator of the primary mass, i.e., heavier nucleus shows larger  $N_\mu/N_e$  around the shower maximum [30].

Moreover, the shower generation and development has intrinsic fluctuations because the particle interaction is a stochastic process. The fluctuation is mostly resulted from the first few interactions of the shower. As a result, showers of the same CRs, with the same energy and composition, show a distribution of  $N_\mu/N_e$  instead of a constant. Besides, the scatter of the fluctuation is also dependent on the primary mass, with proton showers being more fluctuating while those of heavy nuclei showing less fluctuation, due to the averaging effects of more nucleons. Therefore, the width of the  $N_\mu/N_e$  distribution is determined by the primary composition.

The  $N_\mu/N_e$  distribution encapsulates the primary composition by both its shape and mean (or peak) value. Figure 1 shows the simulated  $N_\mu/N_e$  distribution in the reconstructed energy bin of 0.5–0.8 PeV, assuming a CR composition model, namely the H3a composition model [31], which is a three-spectral-component fit to observed CR spectra with rigidity-dependent cutoffs. The distributions of each mass group, along with the total distribution, have been shown. Despite of the fluctuation due to the low statistics in the simulation on the left and right ends of the distribution, it is clearly shown that the distributions of each mass group differ from each other in two aspects, corresponding to the shower development. First, the peaks of five mass groups are well separated.

Statistically, the proton showers tend to have the smallest  $N_\mu/N_e$  values, dominating the total distribution at the low-value end. The Fe showers have the largest  $N_\mu/N_e$  ratio, dominating the high-value end of the total distribution. The peak position reflects the most probable value of  $N_\mu/N_e$  for each mass group, which results from the fact that heavy nucleus produces more muons than the light nucleus. Second, the width of the distributions is different between mass groups. The proton showers disperse over a wider range compared to heavier nuclei, whereas the Fe distribution is narrower, resulting from smaller fluctuations of the development of Fe shower.

The fact that different mass groups are well separated in  $N_\mu/N_e$  distribution allows for decomposing CR compositions and reconstructing the elemental energy spectra by fitting  $N_\mu/N_e$  distribution, as discussed in the following.

### C. Derivation of fluxes for different mass groups

In our approach, we generate template  $N_\mu/N_e$  distributions for individual mass groups by MC simulation, with which we decompose the observed  $N_\mu/N_e$  distribution into different mass groups, and then reconstruct the elemental energy spectra. The events of both observed data and MC are binned in  $E$  and  $N_\mu/N_e$ . We fit the observed  $N_\mu/N_e$  distribution independently in each energy bin with the template distributions. The fluxes of different mass groups in a given energy bin are given by the best fit. Therefore, the elemental energy spectra of CRs are reconstructed by fitting the fluxes of the five mass groups in separate energy bins.

Note, we use the template  $N_\mu/N_e$  distributions of individual mass groups coming from MC simulation rather than doing any parameterization of the distribution. It is necessary to assume a *template model* for the spectral shape of each mass group within one energy bin. However, see discussion in section IV B, the choice of the template model and hence the spectral shape could have little effect on the fitting results, because of the narrow binning of energies. Thus, the MC simulated templates can well describe the profile of the distribution for each mass group at given energy. Moreover, we also note that the fitting is done independently for energy bins, so that the method is CR composition model independent, avoiding circular reasoning in measuring CR compositions.

Therefore, the free parameters in the fitting of the observed total distribution are only the fluxes of individual mass groups, here denoted as the normalization factors  $f^k$  with respect to the assumed flux for the each mass group, where  $k$  stands for the nucleus types. For the best-fit of  $f^k$ , the flux of nucleus  $k$  is derived to be  $f^k F_0^k(E_i)$ , with  $F_0^k(E_i)$  being the assumed flux at energy  $E_i$  when generating the template distributions.

To obtain the best fit, we use Markov chain Monte Carlo (MCMC) implemented in Ref. [32] to sample the distribution of likelihood. The best fit value is the median

TABLE I: Three MC tests.

Test	Input model	Template model
I	GSF	H3a
II	GSF	PG
III	PG	H3a

Note, template model is assumed to generate the template  $N_\mu/N_e$  distributions of individual mass group, and input model to generate the mock observational data.

value of the *a posteriori* distribution and the statistical uncertainty is bracketed by the 16% and 84% percentiles. Detailed fitting procedure is described in App. B.

#### IV. MONTE CARLO TEST

In the following, we carry out MC simulation to test the validity of the composition measurement approach proposed in section III, and derive the uncertainty of the reconstructed elementary spectra. The observational data is replaced by the mock data from MC simulation assuming a certain *input composition model*, thus the mock data will be fitted with the procedures described in Sec. III C. The fitting results are compared with the input composition model of the mock data to examine the capability of recovering the CR compositions. In this analysis, we use the same simulation data set for producing the mock data and the MC templates.

In order to estimate the effects of template model and the input model on decomposing the CR composition, the method should be tested under various assumptions. Table I summarizes the three MC tests in this work, showing the input and template composition models. We consider three choices of CR models. Besides the H3a model [31], we take the Global Spline Fit model (GSF), which is the latest empirical fit from the available experiment data [33], and the Poly-gonato (PG) model [34], which is also empirical fit of observed data, assuming rigidity-dependence for spectral cutoffs of different nuclei. We only consider the five leading mass groups for simplicity: proton, He, CNO, MgAlSi, and Fe. The simulation of CNO (MgAlSi) mass group is simplified by approximating the mass group by the nucleus in the middle, i.e., N (Al), whose flux is the summation of the three nuclei in the mass group.

##### A. Benchmark test

For the benchmark test, Test I, the template CR composition model is taken to be H3a model for the template  $N_\mu/N_e$  distributions of individual mass groups, and the input CR composition model is taken to be GSF model for the mock data distribution. The results of the benchmark test (Test I) are shown in this section, which is followed by the other tests with the input or template

model changed to estimate the effects of the model assumptions.

The events are binned in  $E$  and  $N_\mu/N_e$  in log scales. The energy range of this analysis is  $E = 0.2 - 20$  PeV. This wide energy range helps to better probe the composition evolution around the knee and the possible spectral breaks of elemental energy spectra. The energy is binned in log space,  $\log(E/\text{GeV})$ , with a step size of 0.2, in comparison with the energy resolution of better than 15% above 300 TeV. The  $N_\mu/N_e$  ratio is evenly binned in log space with a step size of 0.025 in the range of  $N_\mu/N_e = 10^{-1.5} - 10^{0.5}$ , which is a compromise between the number of bins and the statistic within each bin.

Presented below are the fitting results of  $N_\mu/N_e$  distribution and the reconstructed elemental energy spectra and discussions on uncertainties.

##### 1. Best fit of $N_\mu/N_e$ distribution

The flux of each mass group is fitted by maximizing the likelihood of observing the mock  $N_\mu/N_e$  distribution. The template distributions of the five mass groups are adjusted vertically in the y-axis, i.e., fitting the fluxes of the mass groups, to find the parameters that maximize the likelihood. Figure 2 shows, for example, a case of the best fit result for the  $N_\mu/N_e$  distribution in the energy bin of 0.5–0.8 PeV. The upper panel shows the  $N_\mu/N_e$  distribution of the mock data and the best fit distribution, as well as the contributions from each mass group. The bottom panel shows the ratio between the best fit distribution and the mock data. One can see the best fit well restores the  $N_\mu/N_e$  distribution.

It should be noted that in the MC test, the used template model, i.e., the assumed spectral shape within an energy bin, is different from the input model for the mock observational data. The good recovery of the ratio distribution suggests the insensitivity of the fitting to the template model.

However, the statistical uncertainty affects the uncertainties of the fitted fluxes, which is mainly from the limited MC sample size. In the energy bin of 0.5–0.8 PeV, the peak region of the  $N_\mu/N_e$  distribution, with  $0.1 < N_\mu/N_e < 0.3$ , is better sampled with smaller statistical uncertainties, whereas the side wings of the distribution have less statistics and thus larger fluctuation. For example, Fig. 2 shows the right wing ( $N_\mu/N_e > 0.4$ ) is underestimated by the fitting, where the Fe group dominates the distribution. At higher energies, the fitting is more biased to the peak region of the  $N_\mu/N_e$  distribution while the side wings are increasingly underestimated, compared to the mock data.

##### 2. Reconstructed elemental energy spectra

The elemental energy spectra are reconstructed by fitting the  $N_\mu/N_e$  distributions binned in primary energy.

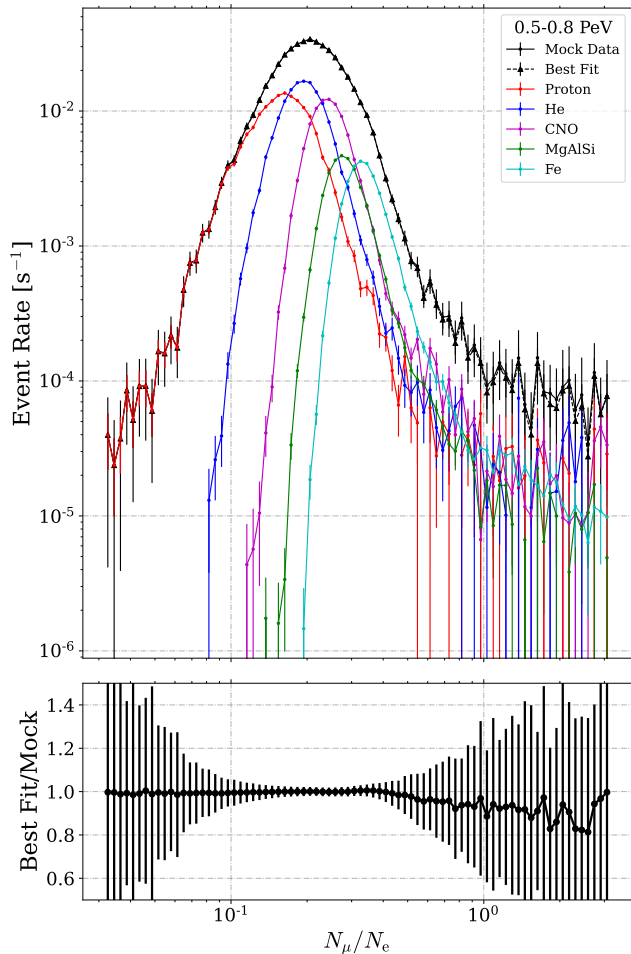


FIG. 2: The best fit of  $N_\mu/N_e$  distribution in the energy bin of 0.5–0.8 PeV (Test I). Upper panel: The mock data with GSF model (black solid line); the best fit (black dashed line); and the template distributions of individual mass groups with the H3a model: proton (red), He (blue), CNO (magenta), MgAlSi (green), and Fe (cyan). Lower panel: the ratio between the best fit distribution and the mock data. The error bars are the statistical uncertainties due to limited simulated samples.

The reconstructed energy spectra of the five mass groups from 0.2 PeV to 20 PeV are shown in Fig. 3, along with the input CR model, GSF, for comparison. The derived fluxes are the median values of the a posteriori distributions sampled by MCMC. The profiles of elemental energy spectra are well reconstructed in general.

The ratios of the best fit fluxes and the input model GSF are shown in Fig. 4 for the five mass groups. The GSF model is basically within the  $1\sigma$  range of the reconstructed spectra. The reconstructed fluxes of all mass groups are well matching the input model.

Overall, the bias of the reconstructed spectra is small, while the deviation also differs for mass groups. The

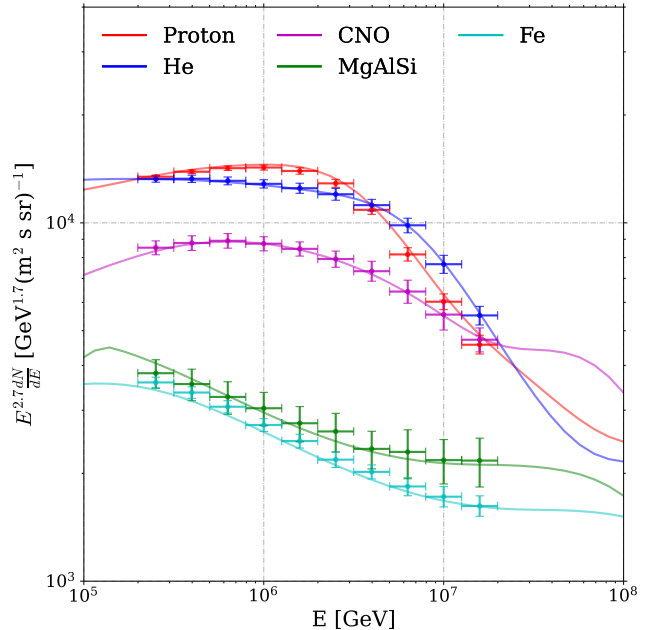


FIG. 3: Reconstructed elemental energy spectra for GSF model in Test I. Different colors represent different mass groups, as annotated in the figure legend. The data points show the reconstructed elemental energy spectra of different mass groups, with the error bars given by the 16% and 84% percentiles of the posterior distributions. In comparison, the solid lines present the input GSF model.

He and CNO spectra are best reconstructed, compared to the other mass groups, with the maximum deviations around 2%. The biases of the reconstructed energy spectra for proton and Fe are within 6%. And the reconstructed MgAlSi spectrum has the largest deviations from the GSF model,  $\sim 7\%$ .

Given that the template and input models are different, the consistency between the reconstructed spectra and the mock data shows that the proposed approach works well to decompose the chemical composition of CRs around the knee.

The anticorrelation between adjacent mass groups is also observed somewhat, e.g., the underestimate of CNO group in 0.5–1 PeV is correlated with the overestimate of MgAlSi in the same energy bin. The correlation and degeneracy between mass groups will be further discussed in Sec. IV A 3.

### 3. Uncertainties of reconstructed elemental energy spectra

The performance of the proposed CR decomposing method is further evaluated here by the uncertainties of the reconstructed elemental energy spectra. We find that: the uncertainties of the reconstructed spectra depend on both mass group and energy; and there is (anti-

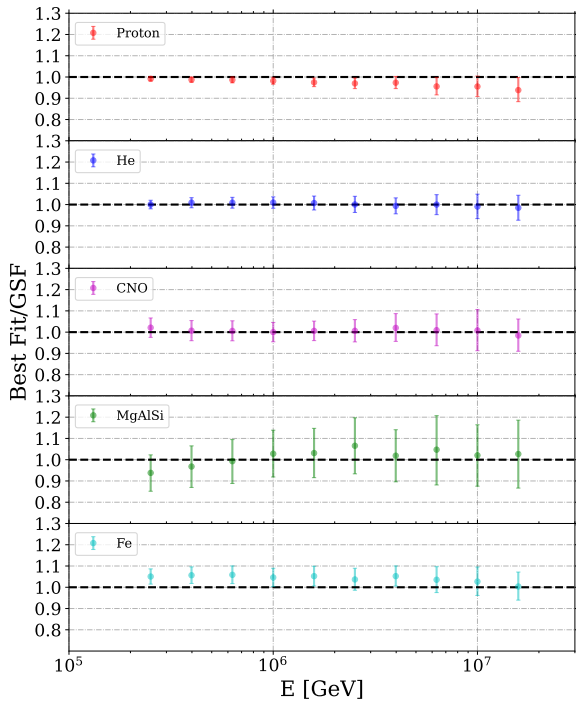


FIG. 4: Ratios between reconstructed fluxes to the input ones as function of reconstructed energy in Test I. From top to bottom shown are for the five mass groups, proton, He, CNO, MgAlSi, and Fe.

)correlation between the fitting results of different mass groups.

As for the composition and energy dependence, one can see, from the fitting results, smaller uncertainty for proton, He, and Fe, but larger for CNO and MgAlSi; and larger uncertainty at higher energy. We show in Fig. 5 the uncertainties of the best fit to the five mass groups in 0.2–20 PeV. For proton and He, the relative uncertainties are 2% at 200 TeV and 6% at 20 PeV; for Fe, the uncertainty increases from 3% at 200 TeV to 7% at 20 PeV. As for CNO and MgAlSi, the uncertainties range from 5% and 9% at 200 TeV to 8% and 16% at 20 PeV, respectively.

The reasons why proton, He and Fe groups are relatively better constrained could be understood. The  $N_\mu/N_e$  distribution is usually a bump with two side wings dominated by the lightest and heaviest mass groups (Fig. 2), thus proton and Fe fluxes are constrained with smaller uncertainties. And He is next to proton in the distribution, with the  $N_\mu/N_e$  peak well separated from the other groups, namely, proton and CNO (see Fig. 2), so the fitting of He flux is less affected by the mixing with proton and CNO groups. On the contrary, the two intermediate mass groups, CNO, and MgAlSi, which lie mostly around

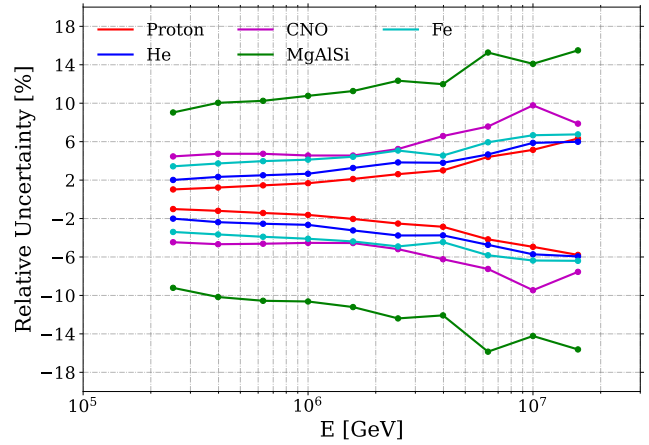


FIG. 5: Relative uncertainties of the reconstructed elemental energy spectra as function of reconstructed energy in Test I. The colorful lines correspond to different mass groups.

the peak region of the distribution, are subject to strong mixing of all the mass groups which makes the decomposition more challenging. Therefore, the determination of CNO and MgAlSi fluxes is less certain.

The reason why the fitting is better at low energies and more uncertain at high energies could be understood too. The dependence on energy of the uncertainty is mostly attributed to the limited MC sample size. Since the MC simulation is sampled from a  $E^{-2}$  power-law, low energy showers are better sampled, while the high energy showers have smaller statistics with larger fluctuations. In principle, a larger simulation library can reduce the statistical uncertainties. However, the simulation of high energy shower is so time-consuming that the dependence on energy of the uncertainty is almost inevitable.

Finally, we find that there is correlation and degeneracy between fitting parameters, i.e.,  $f^k$  (with  $k$  denoting different mass groups, see App. B), reflected by the posterior distributions of the MCMC. Figure 6 shows, for example, the a posteriori distributions and the correlations between the fitting parameters in the energy bin of 0.5–0.8 PeV. The fitting parameters are  $f^k$ 's. The adjacent mass groups are anti-correlated, e.g., CNO and MgAlSi, which results from the overlap between the two adjacent mass groups. The mock data constrains the total number of events contributed by the two (or more) overlapping mass groups which leads to an anticorrelation or degeneracy between neighborhood nuclei. Therefore, the alternate mass groups are positively correlated, e.g., CNO and Fe. The correlation decreases for distant mass groups. For example, proton and Fe have the weakest correlation in Fig. 6, because they are best separated for the  $N_\mu/N_e$  spectrum. The degeneracy between  $f^k$ 's is not unique to this analysis, but ubiquitous for any measurements on the elemental energy spectra.

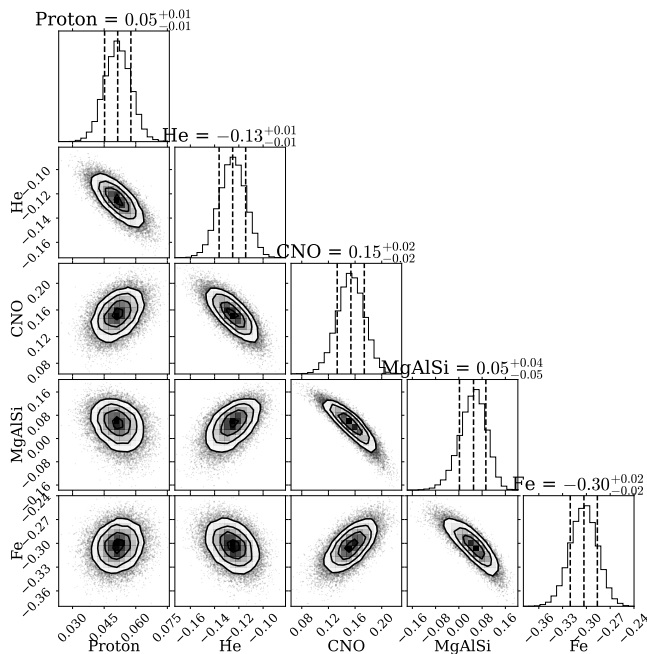


FIG. 6: Posterior distributions and correlations of  $\log f^k$  of the five mass groups in the energy bin of  $0.5 - 0.8$  PeV (Test I).

### B. Test for different template composition model

Since the template distributions of mass groups depend on the presumptions of spectral shapes within the energy bins, i.e., the template model, here we further carry out Test II, in comparison with Test I, to examine the dependence on template models. In Test II, we use the PG model to generate the template distributions, whereas the mock composition is kept the same as Test I. We approximate PG's mass groups of CNO, MgAlSi, and MnFeCo by simulating only the middle nucleus, i.e., N, Al, and Fe, and the nucleus flux is from summing fluxes of all three nuclei within the mass groups. Template distributions of  $N_\mu/N_e$  are produced with the PG model for the five mass groups after the above simplifications.

Figure 7 compares the results of Test II to Test I, under two different template models, i.e., PG versus H3a. The composition reconstruction is robust for changing the template models, where the difference between the two results is smaller than 9%. Particularly, the differences of results obtained with the two template models are within 2% for low energies ( $< 4$  PeV). The largest deviation is the He spectrum above 10 PeV which likely comes from fluctuation caused by the small statistic of the MC sample. On the other hand, the errorbars represent the statistical uncertainties due to the limited simulation sample.

The consistency of the reconstructed spectra with different template models demonstrates the decomposing method is almost independent on the CR composition model. This is because the MCMC fitting is done in-

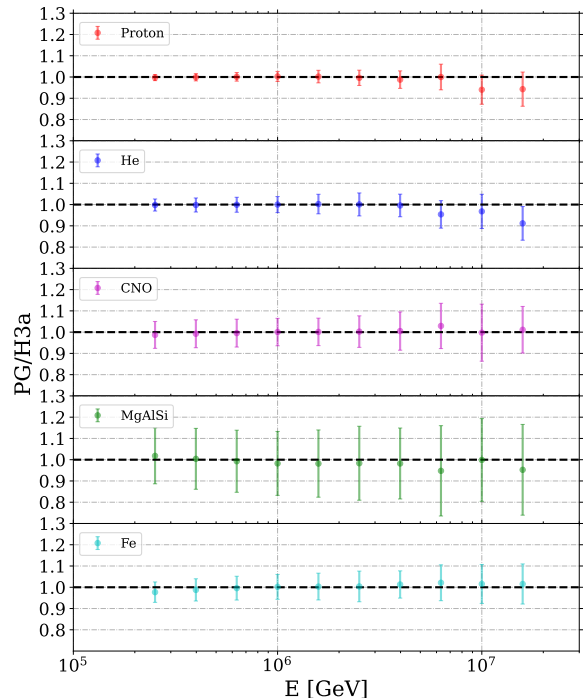


FIG. 7: The ratio between the fluxes resulted from Test II and Test I (PG and H3a as template composition models, respectively) as function of the reconstructed energy. The error bar is only statistic uncertainty.

dependently in each energy bin, and the energy bin is narrow enough so that the template spectral shape does not matter much.

### C. Test for different input composition model

In order to test the reconstruction performance we also try the case of different input composition model. Here we carry out Test III, where, compared to Test I, the input composition model is replaced by the PG model, whereas the the template model is kept the same. The reconstructed energy spectra for PG model are shown in Fig. 8. The knee of proton and He below 10PeV are well restored by the reconstruction. The relative uncertainties are presented in Fig. 9. The reconstruction is done very well, with the reconstructed fluxes consistent with the PG model within the  $1\sigma$  error.

The uncertainty changes very little compared with the results of Test I. For proton spectrum, the uncertainty is 1% at 200 TeV and 9% at 20 PeV. For He and Fe groups, the uncertainties are 2% at 200 TeV and up to 5% at 20 PeV. As for CNO and MgAlSi the uncertainty increases from 7% and 12% at 200 TeV to 9% and 20%



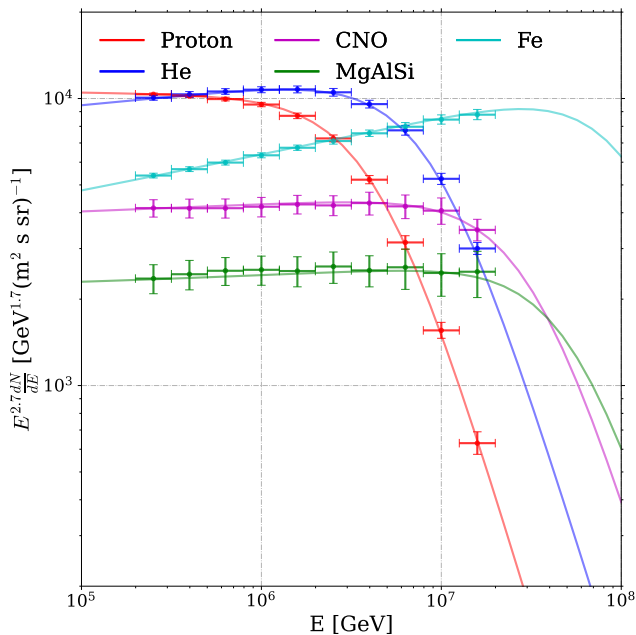


FIG. 8: Same as Fig. 3, but for Test III.

at 20 PeV, respectively.

The dependence of the uncertainties on the mass groups also exists for Test III. Again, the fluxes of proton, He, and Fe are better reconstructed, while the reconstruction of CNO and MgAlSi suffers more degeneracy due to stronger mixing of the two intermediate mass groups.

The good recovery of the elemental energy spectra with a different input model demonstrates the reconstruction method is capable of restoring the CR composition in general, instead of only for certain input models.

## V. SUMMARY AND DISCUSSION

In this work, we propose an approach to reconstruct the elemental energy spectra of CRs around the knee with the  $N_\mu/N_e$  distribution measured by LHAASO-KM2A: the energy spectra of individual CR compositions is obtained by fitting  $N_\mu/N_e$  distributions in each reconstructed energy bin using the template shapes of  $N_\mu/N_e$  distributions of individual CR compositions based on MC simulation. We validate the feasibility of the approach and estimate the uncertainties of the reconstruction with MC test, where we fit the mock data generated by MC simulation to test how well the input composition model can be restored. The uncertainties depend on mass and energy of the primary CR. In Test I using the GSF model as the input composition and the H3a model to generate template distributions, we find that the CR spectra of individual mass groups below 20 PeV can be well reconstructed by LHAASO-KM2A, for proton, He, and Fe groups, with uncertainty  $< 7\%$  below 20 PeV, though somewhat larger uncertainties for CNO

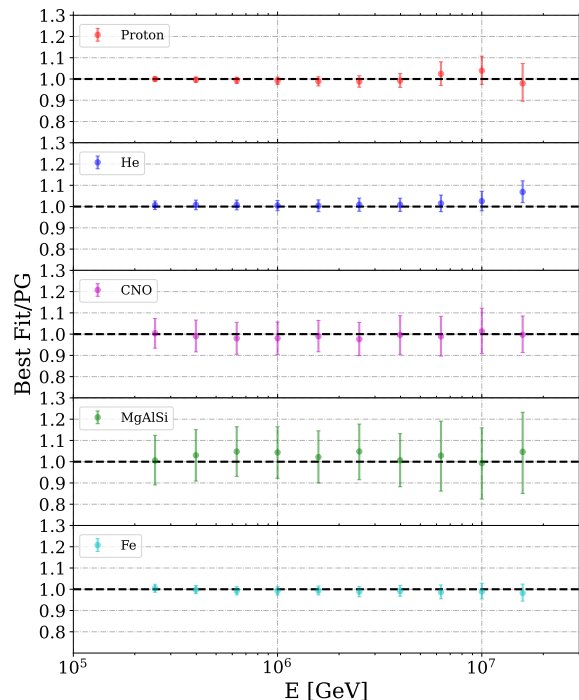


FIG. 9: Same as Fig. 4, but for Test III.

and MgAlSi,  $< 8\%$  and  $< 16\%$  below 20 PeV, respectively. Furthermore, the versatility of the reconstruction is demonstrated by Test II and III where different template and input models are tested, showing good recovery of the input CR spectrum and weak dependence on the template model of individual mass groups.

The consistency with different template models demonstrates the CR model independence of the method. This is mainly because the MCMC fitting is done independently between energy bins. This is especially desirable compared with those methods explicitly involving assumptions on CR composition, and avoids circular reasoning. Some methods using neural network to decompose CR compositions necessitates a presumed composition model for training the network, e.g., hypotheses for proton or heavy dominant [16], or equal mixture among four mass groups [35]. However, the true CR composition distribution likely deviates from the assumption.

We also caveat that the CR model independence of this reconstruction method is at the expense of relying on an accurate description of  $N_\mu/N_e$  distribution for the five mass groups. At low energies, MC simulation has sufficient statistic to sample the expected ratio distribution. At higher energies, the sampling may be incomplete due to poorer statistic, which introduces bias to the fitting. Considering the difficulty of simulation at high energies, parameterizing  $N_\mu/N_e$  distribution from

simulation may overcome the limited MC sample size with introducing acceptable model dependence. For example, KASCADE used parameterization to overcome the insufficiency of simulation and extrapolation to better describe the side wings of  $N_\mu$  distribution that are hard to simulate [15]. IceCube used kernel density estimation to extract the template distributions of the four mass groups [35]. Presently, the template distributions in this analysis are directly from the simulation data without parameterization, which is more based on simulation with minimized model dependence on the choice of the parameterization.

In our method, the template distributions of individual mass groups rely on simulation, thus other uncertainties will arise when applying the method to measurements, i.e., the uncertainties from the hadronic interaction model and the atmosphere model, which is a general problem for decomposing method based on air shower simulation. In future analysis of measurements, more than one hadronic interaction model should be used to estimate the related systematic uncertainties. Moreover, the atmospheric profile could be more properly described. Also, the possible seasonal variation should be considered. On the other hand, one may try to reconstruct the energy and composition together in order to mitigate the potential migration effect, especially for the events with small number of detectors triggered.

## ACKNOWLEDGMENT

This work is supported by the Natural Science Foundation of China (No. U1931201 and No. 12175121) and National Key R&D Program of China No.2023YFE0102300. This work uses the crlfux package [36] to calculate the flux of CR models.

## Appendix A: Event selection

Event selection filters out showers that are poorly reconstructed, e.g. showers with core position outside the array or showers with few secondary particles. On the other hand, the event selection depends on the scientific goal of the analysis to minimize the loss of events of interest. The selection conditions used in this analysis are as follows. (1) The zenith angle of the shower is from  $10^\circ$  to  $30^\circ$ , which is determined by matching the grammage of the atmosphere and the shower maximum of the energy range to be studied. (2) Distance of the shower core from the array center is from 320 m to 420 m to ensure the shower is well contained in the array with a good measurement of the em. and muonic content in the shower. (3) More than 50 EDs are triggered. (4) The number of secondary electromagnetic particles and muons located 40–200 m from the shower axis should be greater than 80 and 15, respectively.

The geometry cut, i.e., cuts on the shower zenith angle and the shower core position, is used to select the showers that are well measured by KM2A array with little particles absorbed in the atmosphere or falling outside the array, which minimizes the bias and uncertainty in the reconstruction. The requirements on the minimum number of em. and muon particles is to guarantee the reconstruction quality. The more secondary particles the array collects, better the reconstruction will be. At the same time, the minimum numbers of muons and electrons determine the threshold energy of the array, which makes the analysis start from 200 TeV.

## Appendix B: MCMC Fitting of $N_\mu/N_e$ distribution

The fluxes of the five mass groups are derived from fitting the  $N_\mu/N_e$  distribution in the reconstructed energy bins. We use MCMC to sample the likelihood distribution of observing the actual data for different compositions, where the best fit maximizes the likelihood.

The events are binned into primary energy  $E$  and ratio  $R \equiv N_\mu/N_e$  bins. We define bin  $(i, j)$  where  $E_i < E < E_{i+1}$  and  $R_j < R < R_{j+1}$ . and  $N_{i,j}^{\text{pred}}$  and  $N_{i,j}^{\text{obs}}$  as the model-predicted and observed numbers of events, respectively, in bin  $(i, j)$ .

For a given composition model, the predicted number of events in a bin should be the sum of the contributions from all mass groups, and can be given by

$$N_{i,j}^{\text{pred}} = \sum_k f_i^k N_{i,j}^{\text{temp},k} \quad (\text{B1})$$

where  $N_{i,j}^{\text{temp},k}$  is the number of event contributed by nucleus  $k$ , with  $k = \text{proton, He, CNO, MgAlSi, or Fe}$ , in bin  $(i, j)$  for the adopted template composition model, and  $f_i^k$  is the normalization factor for nucleus  $k$  and energy bin  $E_i$ .  $f_i^k$  is the parameter to be determined by comparing model with observation.

We assume the number of events in a bin can be approximated by a Gaussian distribution for large event counts. Thus, the likelihood in bin  $(i, j)$  can be given by

$$\mathcal{L}_{i,j}(N_{i,j}^{\text{obs}}|N_{i,j}^{\text{pred}}) = \frac{1}{\sqrt{2\pi}N_{i,j}^{\text{pred}}} \exp\left[-\frac{(N_{i,j}^{\text{obs}} - N_{i,j}^{\text{pred}})^2}{2N_{i,j}^{\text{pred}}}\right], \quad (\text{B2})$$

which depends on the fluxes of the five mass groups. In energy bin  $i$ , the likelihood considering all  $R$  bins is

$$\mathcal{L}_i(N_i^{\text{obs}}|N_i^{\text{pred}}) \equiv \prod_j \mathcal{L}_{i,j}(N_{i,j}^{\text{obs}}|N_{i,j}^{\text{pred}}), \quad (\text{B3})$$

where the right hand side runs over all  $R_j$  bins. Therefore, one can find the best-fit flux of each mass group at energy bin  $i$  by maximizing  $\mathcal{L}_i(N_i^{\text{obs}}|N_i^{\text{pred}})$ .

This can be done in each energy bin to derive  $f_i^k$ 's. The best-fit flux can be given by  $F^k(E_i) = f_i^k F_0^k(E_i)$ , where  $F_0^k(E_i)$  is the flux of nucleus  $k$  at energy  $E_i$  for the

adopted template composition model. Therefore, the elemental energy spectra of each mass group are obtained.

With  $F_0^k(E_i)$  the flux of nucleus  $k$  at energy  $E_i$  for the adopted template composition model, the best-fit flux can be given by  $F^k(E_i) = f_i^k F_0^k(E_i)$ .

- 
- [1] G. Kulikov and G. Khristiansen, On the size spectrum of extensive air showers, *Sov. Phys. JETP* **35**, 441 (1959).
- [2] T. Stanev, P. L. Biermann, and T. K. Gaisser, Cosmic rays. IV. The spectrum and chemical composition above  $10^4$  GeV, *Astron. and Astrophys.* **274**, 902 (1993).
- [3] K. Kobayakawa, Y. S. Honda, and T. Samura, Acceleration by oblique shocks at supernova remnants and cosmic ray spectra around the knee region, *Phys. Rev. D* **66**, 083004 (2002).
- [4] W. Baade and F. Zwicky, Remarks on Super-Novae and Cosmic Rays, *Phys. Rev.* **46**, 76 (1934).
- [5] P. O. Lagage and C. J. Cesarsky, The maximum energy of cosmic rays accelerated by supernova shocks, *Astron. and Astrophys.* **125**, 249 (1983).
- [6] S. Gabici, D. Gaggero, and F. Zandanel, Can supernova remnants accelerate protons up to PeV energies? (2016).
- [7] V. S. Ptuskin, S. I. Rogovaya, V. N. Zirakashvili, L. G. Chuvilgin, G. B. Khristiansen, E. G. Klepach, and G. V. Kulikov, Diffusion and drift of very high energy cosmic rays in galactic magnetic fields, *Astron. and Astrophys.* **68**, 726 (1993).
- [8] A. A. Lagutin, Y. A. Nikulin, and V. V. Uchaikin, The “knee” in the primary cosmic ray spectrum as consequence of the anomalous diffusion of the particles in the fractal interstellar medium, *Nucl. Phys.* **97**, 267 (2001).
- [9] C. Julián, R. Esteban, and N. E. Luis, Turbulent diffusion and drift in galactic magnetic fields and the explanation of the knee in the cosmic ray spectrum, *J. High. Energy. Phys.* **2002**, 033 (2002).
- [10] E. Juliusson, P. Meyer, and D. Müller, Composition of Cosmic-Ray Nuclei at High Energies, *Phys. Rev. Lett.* **29**, 445 (1972).
- [11] J. A. Simpson and M. Garcia-Munoz, Cosmic-ray lifetime in the galaxy: Experimental results and models, *Space. Sci. Rev.* **46**, 205 (1988).
- [12] B. Peters, Primary cosmic radiation and extensive air showers, *Nuovo Cimento* **22**, 800 (1961).
- [13] T. K. Gaisser, T. Stanev, and S. Tilav, Cosmic ray energy spectrum from measurements of air showers, *Frontiers of Physics* **8**, 748 (2013).
- [14] P.A. Zyla *et al.* (Particle Data Group), Review of Particle Physics, *Prog. Theor. Exp. Phys.* **2020**, 10.1093/ptep/ptaa104 (2020).
- [15] T. Antoni, W. D. Apel, A. F. Badea, K. Bekk, A. Bercuci, J. Blümer, H. Bozdog, I. M. Brancus, A. Chilingarian, K. Daumiller *et al.*, KASCADE measurements of energy spectra for elemental groups of cosmic rays: Results and open problems, *Astropart. Phys.* **24**, 1 (2005).
- [16] M. Amenomori *et al.* (Tibet AS $\gamma$  Collaboration), Are protons still dominant at the knee of the cosmic-ray energy spectrum?, *Phys. Lett. B* **632**, 58 (2006).
- [17] B. Bartoli *et al.* (ARGO-YBJ Collaboration, LHAASO Collaboration), Knee of the cosmic hydrogen and helium spectrum below 1 PeV measured by ARGO-YBJ and a Cherenkov telescope of LHAASO, *Phys. Rev. D* **92**, 092005 (2015).
- [18] Z. Cao, D. della Volpe, S. M. Liu, X. J. Bi, Y. Chen, B. D’Ettorre Piazzoli, L. Feng, H. Y. Jia, Z. Li, X. H. Ma *et al.*, The Large High Altitude Air Shower Observatory (LHAASO) Science Book (2021 Edition), *Chin. Phys. C* **46**, 10.48550/arXiv.1905.02773 (2019).
- [19] L. Q. Yin *et al.* (LHAASO Collaboration), Expected energy spectrum of cosmic ray protons and helium below 4 PeV measured by LHAASO, *Chin. Phys. C* **43**, 075001 (2019).
- [20] C. Jin, S. Z. Chen, and H. H. He (LHAASO Collaboration), Classifying cosmic-ray proton and light groups in LHAASO-KM2A experiment with graph neural network, *Chin. Phys. C* **44**, 065002 (2020).
- [21] L. Q. Yin, S. H. Chen, and S. S. Zhang (LHAASO Collaboration), Measurement of the cosmic ray iron spectrum with energy from 100 TeV to 10 PeV by LHAASO, *PoS ICRC2023*, 419 (2023).
- [22] H. Y. Zhang, H. H. He, and C. F. Feng, Approaches to composition independent energy reconstruction of cosmic rays based on the LHAASO-KM2A detector, *Phys. Rev. D* **106**, 123028 (2022).
- [23] F. Aharonian *et al.* (LHAASO Collaboration), Observation of the Crab Nebula with LHAASO-KM2A - a performance study, *Chin. Phys. C* **45**, 025002 (2021).
- [24] X. H. Ma, Y. J. Bi, Z. Cao, M. J. Chen, S. Z. Chen, Y. D. Cheng, G. H. Gong, M. H. Gu, H. H. He, C. Hou *et al.*, Chapter 1 LHAASO Instruments and Detector technology, *Chin. Phys. C* **46**, 030001 (2022).
- [25] D. Heck, J. Knapp, J. N. Capdevielle, G. Schatz, and T. Thouw, *CORSIKA: a Monte Carlo code to simulate extensive air showers* (1998).
- [26] S. Z. Chen, J. Zhao, and Y. Liu, Design of the detector simulation of LHAASO-KM2A, *Nucl. Electron. Detect. Technol.* **37**, 1101 (2017).
- [27] S. Ostapchenko, QGSJET-II: physics, recent improvements, and results for air showers, *EPJ Web of Conferences* **52**, 02001 (2013).
- [28] G. Battistoni, T. Boehlen, F. Cerutti, P. W. Chin, L. S. Esposito, A. Fassò, A. Ferrari, A. Lechner, A. Empl, A. Mairani *et al.*, Overview of the FLUKA code, *Ann. Nucl. Energy* **82**, 10 (2015).
- [29] J. Matthews, A Heitler model of extensive air showers, *Astropart. Phys.* **22**, 387 (2005).
- [30] J. R. Hörandel, Cosmic Rays from the Knee to the Second Knee:  $10^{14}$  to  $10^{18}$  eV, *Mod. Phys. Lett. A* **22**, 1533 (2007).
- [31] T. K. Gaisser, Spectrum of cosmic-ray nucleons, kaon production, and the atmospheric muon charge ratio, *Astropart. Phys.* **35**, 801 (2012).
- [32] D. Foreman-Mackey, D. W. Hogg, D. Lang, and J. Goodman, emcee: The MCMC Hammer, *Publ. Astron. Soc. Pac.* **125**, 306 (2013).
- [33] H. Dembinski, R. Engel, A. Fedynitch, T. Gaisser, F. Riehn, and T. Stanev, Data-driven model of the cosmic-ray flux and mass composition from 10 GeV to  $10^{11}$  GeV, *Proc. Sci. ICRC2017*, 533 (2017).

- [34] J. R. Hörandel, On the knee in the energy spectrum of cosmic rays, *Astropart. Phys.* **19**, 193 (2003).
- [35] M. G. Aartsen *et al.* (IceCube Collaboration), Cosmic ray spectrum and composition from PeV to EeV using 3 years of data from IceTop and IceCube, *Phys. Rev. D* **100**, 082002 (2019).
- [36] A. Fedynitch, J. Becker Tjus, and P. Desiati, Influence of hadronic interaction models and the cosmic ray spectrum on the high energy atmospheric muon and neutrino flux, *Phys. Rev. D* **86**, 114024 (2012).